Influence of growth faults on coastal fluvial systems: Examples from the late Miocene to Recent Mississippi River Delta

Christopher Armstrong [a,*], David Mohrig [a], Thomas Hess [a], Terra George [a,1], Kyle M. Straub [b]

[a] The University of Texas at Austin, Jackson School of Geosciences, USA
[b] Tulane University, Department of Earth and Environmental Sciences, New Orleans, LA 70118, USA

ARTICLE INFO

ABSTRACT

The details of how fluvial systems respond to spatial changes in land-surface subsidence produced by active faulting remain incompletely understood. Here, we examine the degree to which the positioning of individual channels and channel-belts is affected by local maxima in subsidence associated with the hanging walls of growth faults. The channel forms and faults are imaged using a seismic volume covering 1400 km² of Breton Sound and Barataria Bay in southern Louisiana, USA. We look at the consequences of interactions between channels, channel-belts, and faults in late Miocene to Recent strata. More than fifty individual channels that crossed the traces of active growth faults were examined. Of these channels, only three appear to have been redirected by the faults. There also appeared to be no systematic change in the cross-sectional geometries of channels or channel-belts associated with crossing a fault, though the orientation of the channel-belts appears to be more influenced by faulting than the orientation of individual channels. Seven out of ten mapped channel-belts appear to have been steered by growth faults. We propose that channel belts are more likely to be influenced by faults than individual channels because channel-belts are longer lived features, unlikely to shift their overall position before experiencing a discrete faulting event. In addition, the style of influence in the few cases where an individual channel is affected by a fault is different from that of larger systems. While downstream of a fault channel-belts generally become oriented perpendicular to fault strike, the individual channels are directed along the hanging wall of the fault, running parallel to the fault trace. We relate this to the ratio of the length-scale of fault rollover relative to the channel or channel-belt width. Fluvial-fault interactions with higher values for this ratio are more likely to be carried parallel to the fault trace than systems with lower ratio values.

© 2013 Elsevier B.V. All rights reserved.

1. Introduction

A basic principle in the study of interactions between fluvial systems and spatially varying subsidence is that rivers can be preferentially attracted to areas of higher subsidence (Alexander and Leeder, 1987). The potential for variations in subsidence to affect fluvial stratigraphy has been documented in numerous field studies (e.g., DeCelles, 1986; Mack and Seager, 1990; Peakall, 1998; Mack and Leeder, 1999; Peakall et al., 2000). Fluvial sensitivity to subsidence is, however, dependent on the interplay of a number of different factors. In a simulation model of alluvial stratigraphy, Bridge and Leeder (1979) found a strong clustering trend in areas of high tectonic tilting due to a fault-created, transverse floodplain slope. In their model, this only occurred when tilting was maintained for a prolonged period of time. Mackey and Bridge (1995) found that tectonic tilting caused channel-belts to shift away from zones of uplift and towards zones of maximum subsidence.

However, in their model, if the aggradation rate is high enough to keep pace with subsidence, no fault effect was seen. This numerical result for the case of high sediment supply was confirmed experimentally by Hickson et al. (2005). Kim et al. (2010) demonstrated the importance of the relative magnitudes of the tectonic timescale versus channel-avulsion frequency when determining the likelihood that a channel will be redirected by subsidence. In their associated physical experiment, channels were most influenced by variations in subsidence if channel mobility was low relative to the accumulation of significant surface relief via spatially varying subsidence rates.

The majority of previous studies have focused on the effects of large, basin-scale extensional tilting on fluvial systems. Only a few workers have looked at the extent to which local faulting can influence stratigraphy. Maynard (2006) used high resolution 3D seismic data to document fluvial response to the development of a growth fault related rollover anticline. A series of seismic time slices imaged the evolution of a system of narrow (100's of meters wide) channels on the hanging wall side of a growth fault. The fluvial system underwent an increase in sinuosity and avulsion frequency in response to the increase in slope created by faulting. Taha and Anderson (2008) studied channel avulsion frequency within the Brazos River incised valley, Texas, USA. Using

core, radiocarbon, aerial photo, and digital elevation-model data, they examined the effect of tilting due to a growth fault on avulsion history within the valley. Their results showed that a late Pleistocene nodal avulsion point was co-located at a site of active movement on a prominent growth fault.

The present study uses an industry-grade 3D seismic volume to examine the effect of local growth faults on fluvial stratigraphy of the late Miocene to Pliocene deposits of the Mississippi River Delta, as well as the modern channel of the Mississippi River. The seismic volume imaged in this study contains dozens of examples of paleo-channels, channel-belts, and valleys that cross growth faults. Most of these growth faults were active for the entire Miocene to Pliocene interval and continue to be active today (George, 2008) so the fluvial systems crossing these faults may have been subject to significant spatial variations in subsidence.

The interplay between cross stream versus downstream surface gradients has been proposed as a primary control on whether or not fluvial stratigraphy is influenced by lateral differences in subsidence (Peakall et al., 2000; Kim et al., 2010). If the cross-stream slope created by growth faulting is much lower than the downstream slope, then growth faults would not be expected to influence channel behavior. Downstream slopes in this coastal study area are low (around $\frac{1}{10,000}$). Field data (Gagliano et al., 2003) show that short term, localized fault displacement rates can be on the order of 10^2 mm/year. As a result, local cross-stream gradients are likely to be more than one order of magnitude greater than the downstream slope, yet small channels appear relatively insensitive to faulting. As demonstrated by Kim et al. (2010), channel mobility is also an important factor in fluvial sensitivity to

growth fault-created subsidence. If the timescale for channel avulsion is short relative to the frequency of faulting events, then an individual channel may avulse before feeling the effect of a fault. The relative timescales of faulting and channel avulsion appear to be an important control for small channels in this dataset.

In addition to the many small channels, the seismic volume imaged in this study shows ten individual channel-belt systems (with widths ranging from 1.5 km to 4 km) that cross growth faults. The relationship between these larger systems and faults has not been previously addressed. While exact avulsion frequencies cannot be constrained from this dataset, channel-belts are relatively long lived features with avulsion frequencies that are likely lower than those of smaller channels. It follows that for channel-belt systems, the ratio of the timescale of avulsion to faulting is higher than for small channels. This allows the relative importance of timescales on the potential for fault influence on fluvial stratigraphy to be examined.

2. Geological setting of the study area

The 1375 km^2 3D seismic survey is located under Breton Sound and Barataria Bay, Louisiana, USA, approximately 50 km southeast of the city of New Orleans and 50 km northwest of the leading edge of the modern Mississippi River Delta (Fig. 1). The seismic survey clearly images channelized features within deltaic sandstone and mudstone over subsurface depths ranging between 500 m and 2000 m. Paleo-Data, Inc. provided us with biostratigraphic data from five wells within the study area that places the base of this 1500 m depth interval in the latest Miocene and its top in the latest Pliocene (Straub et al., 2009).
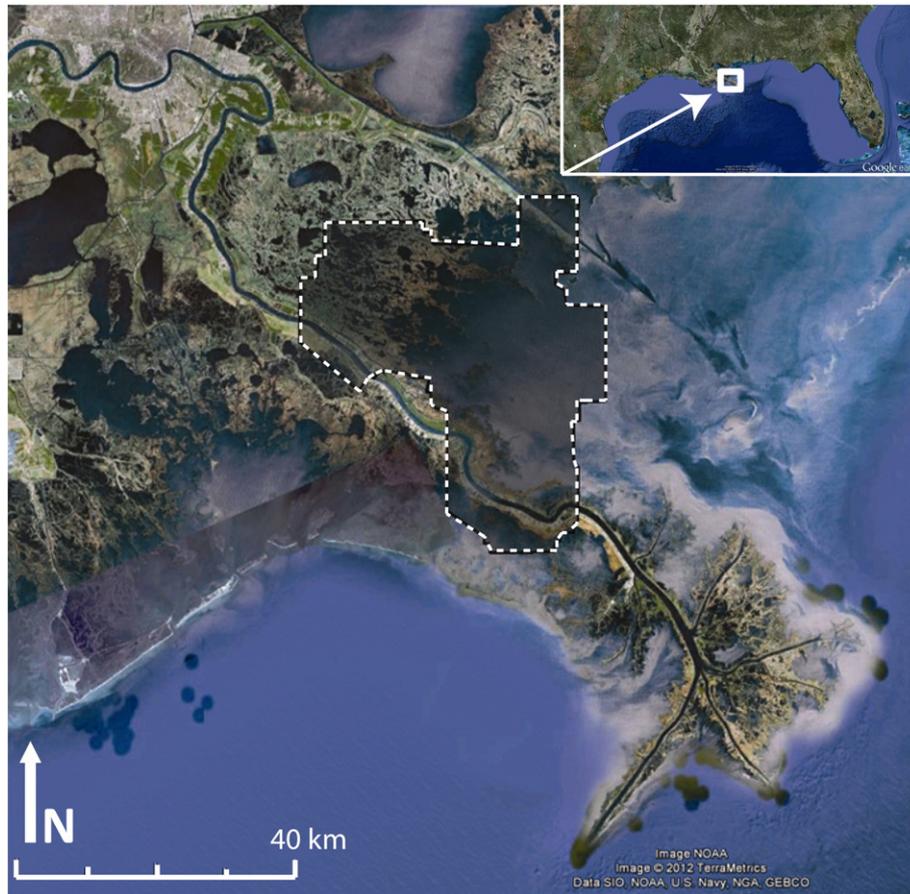

Fig. 1. Aerial extent of the Breton Sound 3D seismic survey outlined on the modern Mississippi River Delta surface (white dashed lines) and regional map showing approximate survey location (white box) along the Gulf Coast. The approximate center of the 3D seismic survey is at latitude 29.468408°, longitude −89.518501° (WGS84 coordinate system). Access to this seismic volume was provided by WesternGeco®; images are satellite photos from Google Earth®.

2.1. Growth faulting

The large volume of terrigenous sediment deposited from the Miocene to Recent has maintained an ensemble of active growth faults within the survey area. Growth strata preserved on the downthrown sides of faults show that these structures are contemporaneous with deposition (George, 2008) and have listric fault planes that flatten with depth. These faults are a result of local, gravity-driven instabilities due to rapid sediment loading and related withdrawal of the Louann Salt (Nelson, 1991). Growth faults are long-lived features and, based on stratigraphic penetration, some can be observed to persist through the seismic volume for in excess of 20 million years. Fig. 2 shows the locations for all of the growth faults present within the upper 1.5 km of the seismic survey.

The seismic volume images approximately twenty-eight growth faults. Most fault planes are from 8 to 12 km wide, dip either basinward or landward, and have roughly east–west oriented strikes. While the amount of surface displacement that existed on a fault at any specific point in geologic time is unknown, modern fault displacements measured within the study area have produced up to 2 m of vertical displacement in the land surface (Gagliano et al., 2003). Fault offsets increase with depth to a maximum value of about 120 m (George, 2008) at 1500 m into the subsurface, near the base of the studied stratigraphic interval. Most of the seismically imaged faults appear to extend up to the modern land surface and some affect the modern delta morphology. Fig. 3 shows mapped fault planes projected onto a satellite photo of the modern delta. As demonstrated by Gagliano et al. (2003) and George (2008) and illustrated in Fig. 3, several of these faults correspond to abrupt shifts from emergent wetlands to fully submerged areas of open water on the delta surface.

The high concentration of both mappable channels and growth faults makes this seismic volume an ideal survey for examining the interplay between fluvial systems and persistent growth faulting. In addition, the range of fluvial styles imaged in the dataset allows for the effect of faults on both small channels and larger fluvial elements to be examined.

3. Methods

3.1. Seismic data

The 1375 km^2 3D seismic volume, consisting of merged surveys covering Breton Sound, Grand Lake, Black Bay, and Quarantine Bay, was acquired by WesternGeco® in 1998 and 1999. Due to the variety of survey environments (from wetlands to shallow open marine), a mix of energy sources was used during survey acquisition including airgun, pentolite, and dynoseis. Seismic processing was completed by WesternGeco® in 2006 and lent to The University of Texas at Austin for research use. Fig. 4 summarizes checkshot results and survey acquisition and processing parameters. All seismic analysis for this project was based off post-stack data. In the ~500 to 2000 m interval of interest, frequency rollover is about 40 Hz (Fig. 5) and P-wave velocities range from 1900 to 2700 ms^{-1} which leads to a best case vertical resolution of about 12 to 16 m. The seismic volume has a sampling rate of 4 ms.
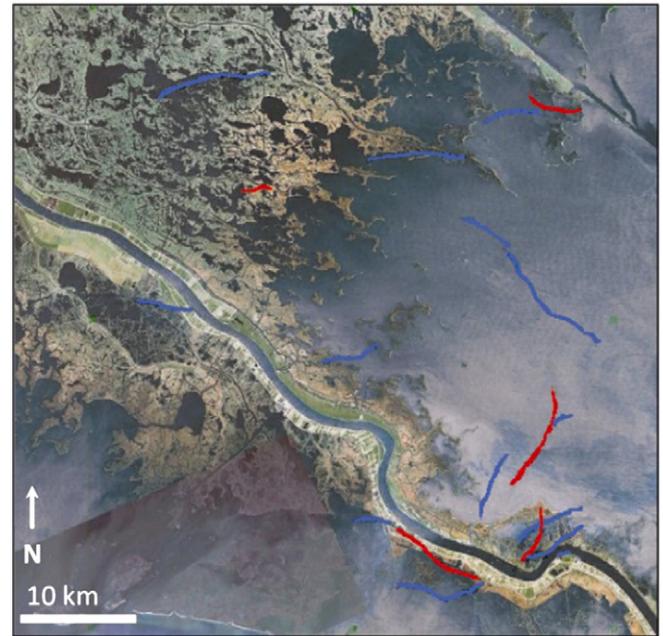

Fig. 3. Projections of fault planes overlain on a satellite photo; blue indicates a basinward fault dip and red indicates a landward dip. See Fig. 1 for regional location.
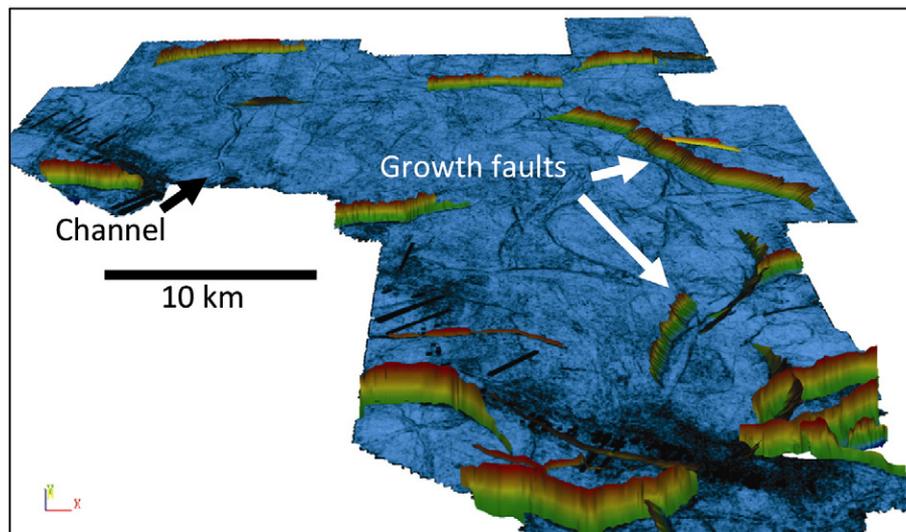

Fig. 2. A perspective view of a horizon slice in the seismic data (looking to the north) showing growth faults within the Miocene to Pliocene survey interval (hotter colors on growth faults indicate shallower depths). The blue surface shows outlines of several north–south oriented late Miocene fluvial systems.
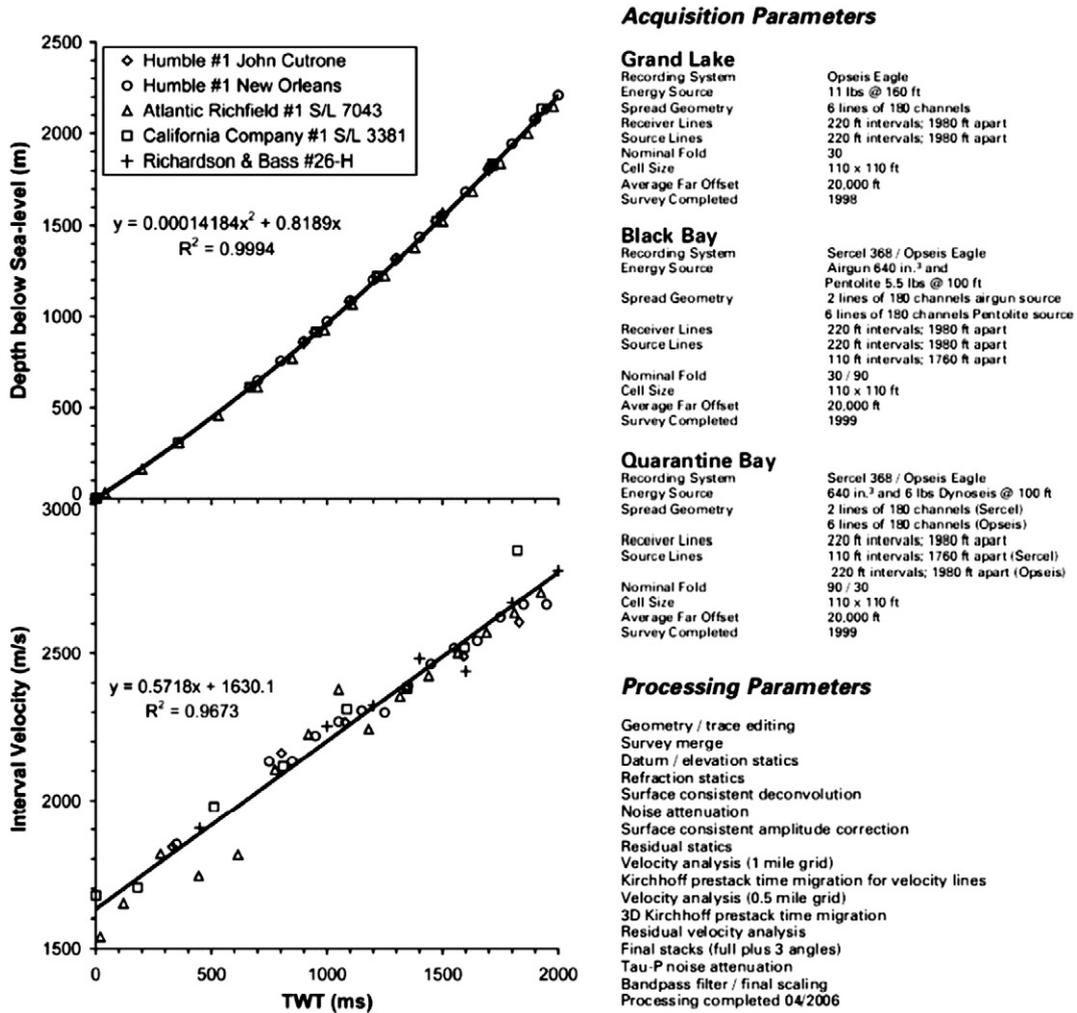
Acquisition Parameters

Grand Lake

Recording System	Opseis Eagle
Energy Source	11 lbs @ 160 ft
Spread Geometry	6 lines of 180 channels
Receiver Lines	220 ft intervals; 1980 ft apart
Source Lines	220 ft intervals; 1980 ft apart
Nominal Fold	30
Cell Size	110 x 110 ft
Average Far Offset	20.000 ft
Survey Completed	1998

Black Bay

Recording System	Sercel 368 / Opseis Eagle
Energy Source	Airgun 640 in.³ and
	Pentolite 5.5 lbs @ 100 ft
Spread Geometry	2 lines of 180 channels airgun source
	6 lines of 180 channels Pentolite source
Receiver Lines	220 ft intervals; 1980 ft apart
Source Lines	220 ft intervals; 1980 ft apart
	110 ft intervals; 1760 ft apart
Nominal Fold	30 / 90
Cell Size	110 x 110 ft
Average Far Offset	20.000 ft
Survey Completed	1999

Quarantine Bay

Recording System	Sercel 368 / Opseis Eagle
Energy Source	640 in.³ and 6 lbs Dynoseis @ 100 ft
Spread Geometry	2 lines of 180 channels (Sercel)
	6 lines of 180 channels (Opseis)
Receiver Lines	220 ft intervals; 1980 ft apart
Source Lines	110 ft intervals; 1760 ft apart (Sercel)
	220 ft intervals; 1980 ft apart (Opseis)
Nominal Fold	90 / 30
Cell Size	110 x 110 ft
Average Far Offset	20.000 ft
Survey Completed	1999

Processing Parameters

Geometry / trace editing
Survey merge
Datum / elevation statics
Refraction statics
Surface consistent deconvolution
Noise attenuation
Surface consistent amplitude correction
Residual statics
Velocity analysis (1 mile grid)
Kirchhoff prestack time migration for velocity lines
Velocity analysis (0.5 mile grid)
3D Kirchhoff prestack time migration
Residual velocity analysis
Final stacks (full plus 3 angles)
Tau-P noise attenuation
Bandpass filter / final scaling
Processing completed 04/2006

Fig. 4. The relationships between two-way travel time (TWT) and interval velocity and TWT and depth below the present-day surface derived from 5 checkshot wells in the study area (George, 2008). Seismic acquisition and processing parameters are also shown here.

3.2. Mapping channels and channel-belts

To define the planform geometry of a channel or channel-belt, a pointset is first created using the digibrush tool in Landmark Geoprobe™ software that defines the edges of the channelized feature along the entire length of the channel. With the feature's edges defined, the pointset can then be converted to a surface and unflattened to bring it to a configuration that agrees with the original seismic volume. This
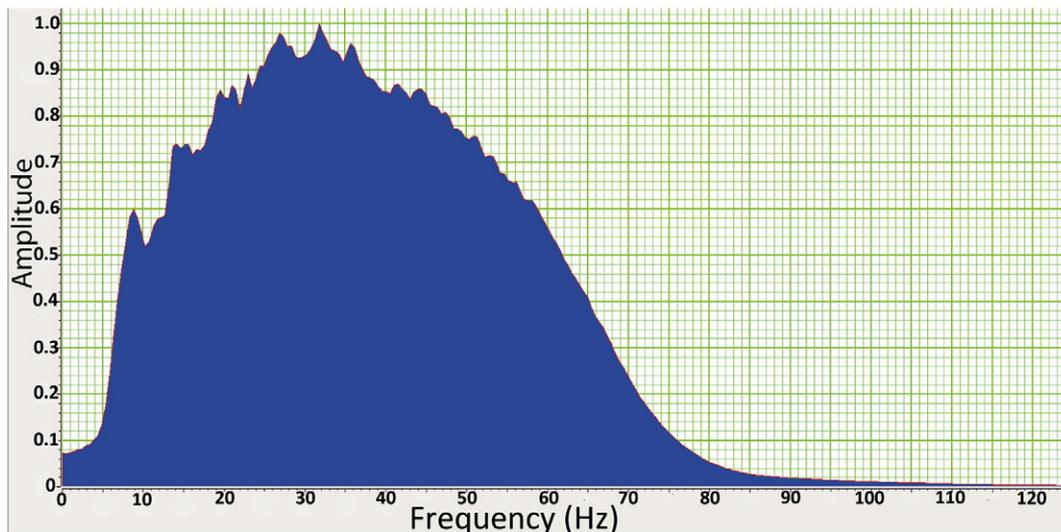

Fig. 5. Amplitude spectrum for the seismic volume from approximately 500 m to 2000 m below the present-day surface. Frequency content peaks at about 35 Hz and begins to decrease rapidly above 45 Hz.

process gives the planform geometry of the channel or channel-belt and allows width, distance along channel, curvature, slope, and sinuosity to be calculated by recording the coordinates of channel boundaries at consistent intervals along the channel centerline. This interval was never greater than one to two times the width of the channelized feature being measured. Estimates of channel or channel-belt thicknesses were obtained by defining the difference in time between the roof of the channel or valley and the thalweg at the same cross section locations where width was recorded. Then, using time versus depth relationships, time was converted to actual thickness and the width to depth ratio was calculated. No attempt to correct for compaction was made for thickness measurements. Similar to channels in Mohrig et al. (2000), fluvial deposits in this dataset are primarily sandy and therefore differential compaction effects are not expected to significantly modify channel geometry in this depth interval. This expectation is supported by the analysis of porosity logs from wells in the study area. These logs record a great deal of local variability in porosity, but the mean reduction in porosity of sand-rich deposits between the land surface and the base of the subsurface interval is less than ten porosity units. Additionally, regional dips are low in the survey (slope of around $\frac{1}{10,000}$) so any difference in measured vertical thickness versus stratigraphic thickness is assumed to be insignificant.

These techniques provide measurements for fluvial geometry as it is preserved in subsurface data. The preserved stratigraphy, however, does not necessarily represent a fluvial system that existed at any specific point in time. Fluvial stratigraphy is the composite, time-transgressive result of erosion and sedimentation. Large fluvial systems imaged in seismic data may be the result of a large channel, the lateral migration of a small channel over a long period of time, or the result of a number of small, concurrently active or superimposed channels. Additionally, seismic imaging of channels is based on variations in acoustic impedance which may be caused by a number of factors unrelated to fluvial cut and fill processes (changes in pore pressure, changes in fluid content, the presence of fractures, etc.). If a fluvial system's fill is similar to the surrounding lithology, then there may be no change in amplitude across its boundary and it will not be clearly imaged. These caveats aside, the continuous (i.e., contiguous and mappable over several tens of kilometers) nature of fluvial systems in this dataset provides strong evidence for the robustness of this 3D seismic based fluvial analysis.

3.3. Measuring fault and channel-belt relationships

Relationships between faults and channel-belts were examined by measuring any changes in paleo-flow direction as the channel-belt crossed the fault (Fig. 6). Change in channel-belt orientation was measured normal to the fault strike at the channel-belt midpoint along the fault trace. The angle defining any difference between the orientation of the normal to fault strike and the direction of the channel-belt was measured over a distance equal to one channel-belt width both upstream and downstream of the fault. The difference between the upstream and downstream angles was then calculated, producing a measure of the change in channel-belt orientation across the fault, which is referred to as the channel-belt reorientation angle (Fig. 6).

A measure of the magnitude of faulting at each channel-belt location is needed in order to compare the effect of faults on channel-belt systems over differing spatial and temporal intervals. Here this is done using the offset ratio: the local vertical displacement on the fault divided by the depth beneath the present-day surface where this displacement and channel-belt were measured (Fig. 7). Because fault displacement increases roughly linearly with depth (George, 2008), the offset ratio provides a way to compare displacements throughout the ~1500 m studied interval.

4. Data analysis

4.1. Distinction of channels and channel-belts in the seismic volume

Both individual channels and broader channel-belts were identified in the seismic data. These are distinguished by dimension (width and depth) and planform shape. Fig. 8 shows an example of both an individual channel element and a channel-belt imaged in the seismic data as well as a modern Mississippi River analog for channel-belt development. The individual channel (Fig. 8A) averages about 200 m in width and 20 m in depth. Channel-belts are significantly larger than individual channels and appear to be a result of lateral channel migration that over time can lead to a "scoop-shaped" planform character as preserved in the seismic data (Fig. 8B). An analog for this planform geometry can
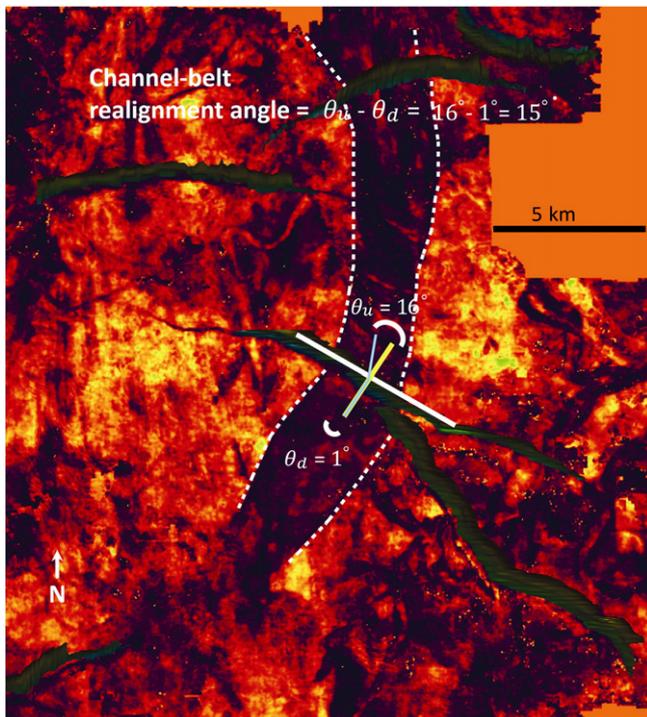

Fig. 6. Definition of channel-belt realignment angle measured at a fault crossing. The orientation of the channel-belt relative to the strike of the fault is measured both upstream, Θ_u, and downstream, Θ_d, of the structure. View (of channel-belt on a horizon slice in the seismic data) is from directly overhead; channel-belt is located in the NE portion of the survey approximately 1.5 km below the present surface.
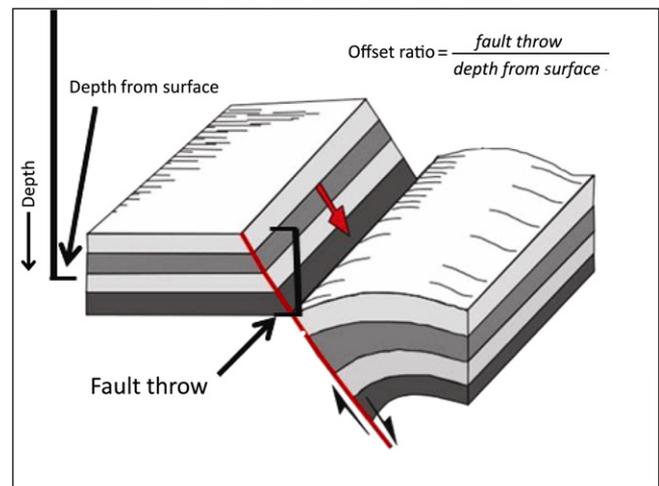

Fig. 7. Definition of offset ratio (from Gagliano, 2005). In the case where fault throw increases roughly linearly with depth, the offset ratio provides a simple way to compare the magnitude of faulting at different depths within the survey.
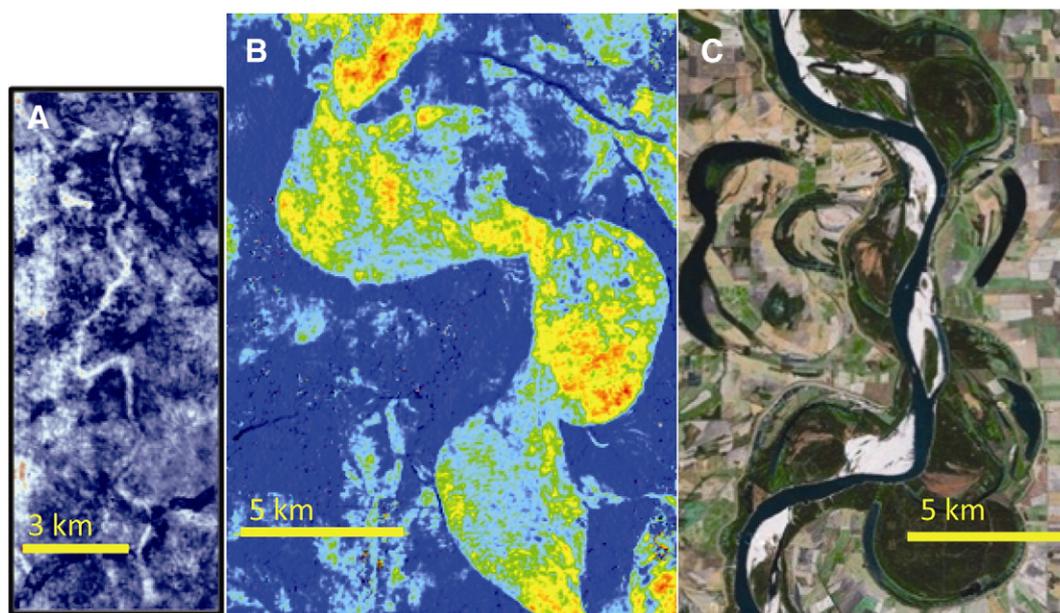
Fig. 8. Examples of channel and channel-belt fluvial styles. A) A north–south oriented channel approximately 200 m wide (from the seismic survey). B) A channel-belt ranging from approximately 2 to 4 km in width (from the seismic survey). C) A modern analog (the Mississippi River in southwestern Arkansas) for the formation of a channel-belt (satellite image from Google Earth®).

be seen in the modern Mississippi River a few hundred kilometers upstream of the survey area (Fig. 8C).

Fig. 9 presents an overview of the geometry of channelized deposits in the seismic volume. The average width and depth (i.e., thickness) were calculated for forty-three fully mapped channelized fluvial elements. Width ranges from around 67 to 31,000 m and depth ranges from 11 to 90 m. When plotted (Fig. 9), the channelized bodies from this dataset follow a power-law scaling relationship between width and depth. Trend-lines for the minimum and maximum width and depth are also derived from the dataset. These show that upper and lower limits on fluvial geometry follow a similar power law scaling relationship.

Previous work (Mohrig et al., 2010) and this study examined the relationship between individual channels (with 75% of measured widths falling below 400 m and 90% falling below 1 km) and growth faults. The results show that geometry (width and depth) and planform for the majority of the mapped channels that intersect growth faults are not affected by them. The width and depth for all of the 54 mapped

paleo-channels do not appear to have been affected by the faults in a systematic way. Fig. 10 shows variations in width to depth ratio for 11 cases of channels and channel-belts that cross faults. Notice that there exists considerable natural variability in channel-elements' width/depth (W/D) measurements with distance downstream. The minimum and maximum values for coefficient of variation (standard deviation/mean) in W/D for the 11 cases are 0.11 and 0.46, respectively, with both the mean and median values for the coefficient of variation in W/D being 0.30. Recognizing these naturally occurring variations in W/D, it is clear to us that there is no systematic variation in width to depth ratio connected to the channel-elements crossing growth faults. Neither the individual channels nor the channel-belts appear to change their cross-sectional shape in response to movement across a fault.

Descriptions of one small channel (Case A) and seven large subsurface fluvial systems (Cases B–H) are presented in this section. All of these subsurface cases intersect and appear to be affected by one or more growth faults.
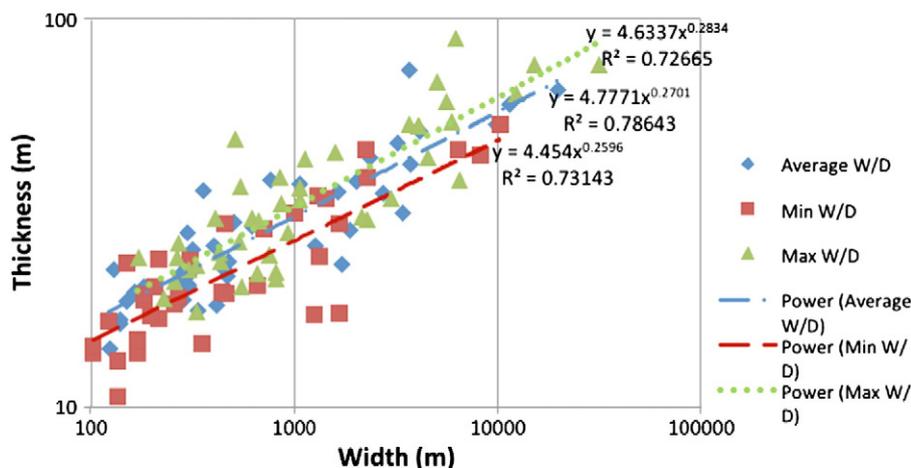

Fig. 9. Width (W) and depth (D) (i.e., channel or channel-belt thickness) average, minimum, and maximum values for forty-three fully mapped examples of fluvial stratigraphy in the seismic dataset.
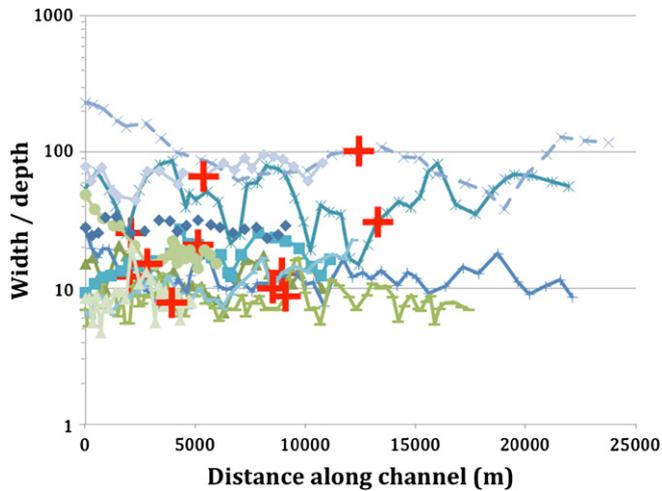
Fig. 10. Width to depth ratio versus distance for 11 cases of channels or channel-belts that cross growth faults (where each colored line represents a different channel or channel-belt). The red plus signs show where growth faults intersect the channels or channel-belts. No systematic change in geometry is evident across the faults.

4.1.1. Case A

Fig. 11 shows a rare example where positioning of a small channel appears to be influenced by a fault. Case A is a narrow (average channel width is 120 m), Pliocene age channel located in the eastern portion of the seismic survey. For a streamwise distance of several kilometers upstream of the fault, the channel has a low sinuosity of 1.09. Less than 50 m downstream of the fault crossing, the channel abruptly turns and flows parallel to the downthrown edge of the hanging wall for a distance exceeding 500 m before turning sharply back into the regional transport direction. The average measured channel width is 120 m and we observed no systematic change in either width or channel-fill thickness across the fault zone. Upstream of the fault, the channel position is approximately 780 m beneath the land surface; downstream of the fault, the channel is approximately 822 m beneath the surface. The fault offset ratio with this 42 m of accumulated channel

Fig. 11. A narrow Pliocene channel aligned with the downthrown side of a mapped fault. The two probes (rectangular boxes) show the channel planform as it appears in the amplitude volume. View is from directly overhead (2D view); hotter colors define shallower depths for the fault plane which is dipping to the left-hand side of the figure.

displacement is about 5%. Overlaying the channel on the time-structure map for the connected stratal slice (Fig. 12) shows that the redirected segment of channel is positioned directly over the subsidence maximum on the downthrown side of the fault. The channel turns out of the fault zone upon reaching a local topographic high labeled point 1 on Fig. 12 and then moves through a relative topographic low between high points 2 and 3 in Fig. 12. A second example of an individual channel position right at the edge of a growth-fault hanging wall is shown in Fig. 13. This spatial correlation between channel and fault position and the time-structure maps estimating the positioning of relative highs and lows in surface topography make up the best evidence we have for individual channels being redirected by local change in land-surface elevation tied to growth faulting.

4.1.2. Case B

This southwest-trending Miocene age channel-belt is located in the eastern portion of the seismic survey and was mapped for over a 19 km distance (Fig. 14). Over the studied section, the channel-belt has a low sinuosity of 1.08, an average width of 2.7 km, and an average fill thickness of 35 m. The channel-belt is completely cut by one southeast striking growth fault and partially intersects a second growth fault that cuts the eastern side of the channel-belt about 200 m downstream from the main fault. Only the relationship between the channel-belt and the main fault is considered here. The channel-belt approaches the fault zone at an angle of 15° from the normal to strike of the fault and exits the zone oriented about 2.5° from the normal to the strike of the fault. The width of the channel-belt is also observed to increase by about 600 m when crossing the fault. The channel-belt crosses the fault at a depth of approximately 1800 m and is displaced 62 m for an offset ratio of 3.4%.

4.1.3. Case C

Case C is a late Miocene channel-belt located in the central portion of the seismic survey and mapped for over a distance of 21 km (Fig. 15). The channel-belt has an overall sinuosity of 1.2 and crosses an east–west trending counter-regional growth fault near the center of the mapped reach. The channel-belt approaches the structure at a 40° angle from the normal to the strike of the fault and leaves the fault zone oriented approximately 14° from normal to the strike of the fault. The channel-belt also increases in width across the fault from an average of 550 m upstream to 970 m downstream of the structure. No corresponding change in fill thickness is resolved. The channel-belt crosses the fault at a subsurface depth of approximately 1600 m and its two segments are offset across the fault by a vertical distance of 75 m, yielding an offset ratio of 4.7%.

4.1.4. Case D

This south trending, late Miocene low-sinuosity channel-belt (Fig. 16) is located in the central portion of the survey and crosses two growth faults about 15 km apart. The fault to the south has no apparent effect on the channel-belt. This may be because the fault only intersects the western-most portion of the channel-belt. The fault to the north, however, does seem to influence channel-belt positioning across structure. The channel-belt approaches the structure at an angle of 12° from normal to the strike of the fault. Downstream of the fault the channel-belt is oriented less than 3° from perpendicular to the strike of the fault. In the vicinity of the fault there is a slight narrowing of the channel-belt, from a width of 1400 m upstream to a width of 1200 m near the structure. As with previous cases, there is no apparent change in fill thickness across the fault. The channel-belt crosses this fault at approximately 1300 m depth and displacement across the fault is 33 m giving an offset ratio of 2.5%.
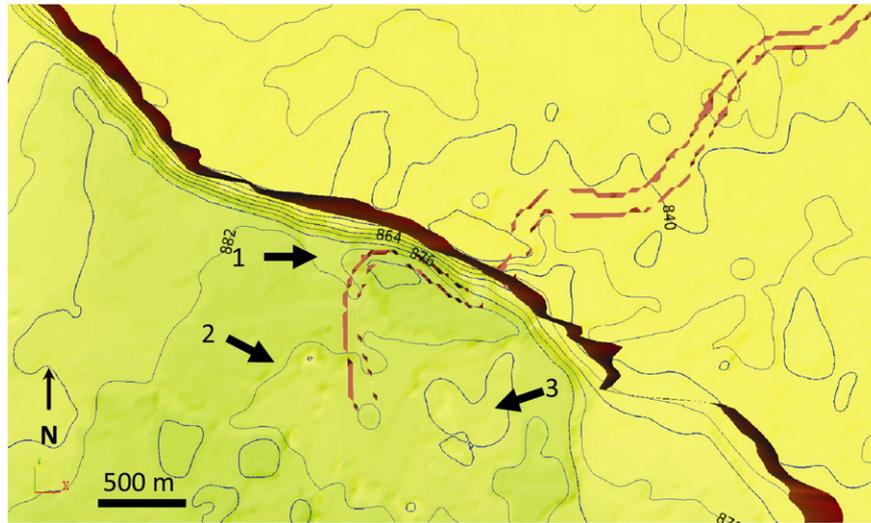
Fig. 12. Time-structure map of a surface that images the channel (map constructed from the seismic data). Numbered points indicate topographically high areas on the hanging wall of the mapped fault (shown here in brown striking northwest–southeast). Contour interval is 6 ms; yellows are high. View is from directly overhead.

4.1.5. Case E

Case E is a south trending Mio-Pliocene channel-belt located in the eastern portion of the dataset and mapped over a 20 km distance. Average width is about 2000 m and average fill thickness is about 38 m. The channel-belt widens in the downstream direction until it bifurcates into a narrow western segment and a wider eastern segment near the southern end of the mapped area (Fig. 17). The channel-belt is fully intersected by two faults, one near its northern end, at about 1415 m below land surface and one near the center of the mapped segment, at a depth of about 1530 m. Vertical offset of the channel-belt by the northern fault is 44 m and channel-belt offset across the southern fault is 64 m, leading to offset ratios of about 3 and 4%, respectively. Upstream of the bifurcation, the channel-belt is very straight and trends almost directly to the south while the faults strike roughly east–west, with the southern fault having a more southeast–northwest oriented strike. Measurements show some redirection of the channel-belt by the faults. For the northern fault, the channel-belt approaches at 5° and leaves at about 4° from normal to the strike of the fault. For the southern fault, the channel-belt approaches at 38° and leaves at 29° from normal to the strike of the fault. This redirection of the channel-belt by the southern fault occurs even though the

channel-belt crosses near the western edge of the fault where its displacements become very low.

4.1.6. Case F

This south trending late Miocene to earliest Pliocene age channel-belt is located in the west portion of the dataset and was mapped over a 20 km distance (Fig. 18). The channel-belt has low sinuosity (1.16) and average width of 2800 m with an average thickness of about 19 m. At about 1330 m depth, the channel-belt is intersected by one east–west trending fault near the northern end of the channel-belt. For a distance of about one channel-belt width upstream of the fault, the channel-belt approaches the fault at an angle of about 21° normal to the strike of the fault. For the same distance downstream of the fault, the channel-belt is oriented less than 6° from normal to the strike of the fault. There is no systematic change in channel-belt width or thickness
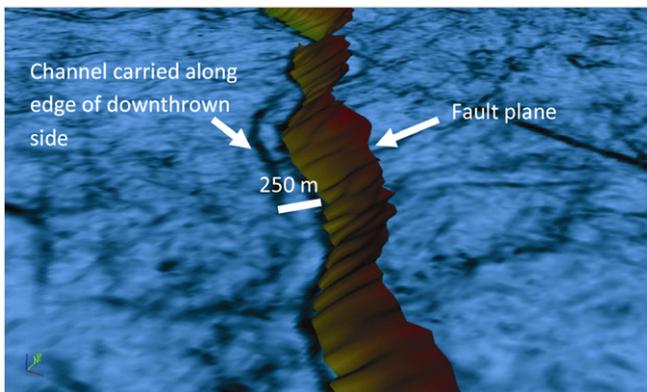

Fig. 13. Perspective view of a narrow channel aligned with the hanging wall of a growth fault for a distance exceeding 1 km. The growth fault is dipping to the left (red indicates shallowest level of the mapped fault). The channel is imaged here on a similarity attribute stratal slice from the seismic data.
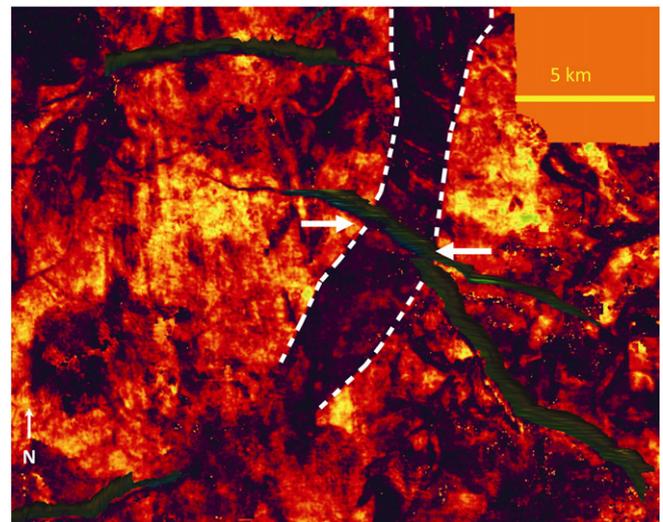

Fig. 14. Case B, a Miocene channel-belt system (dashed lines). View is from directly overhead with sweetness attribute shown. Hotter colors indicate higher sweetness. Arrows point to the fault with the channel-belt imaged as the dark, NNE–SSW aligned area between the two arrows.
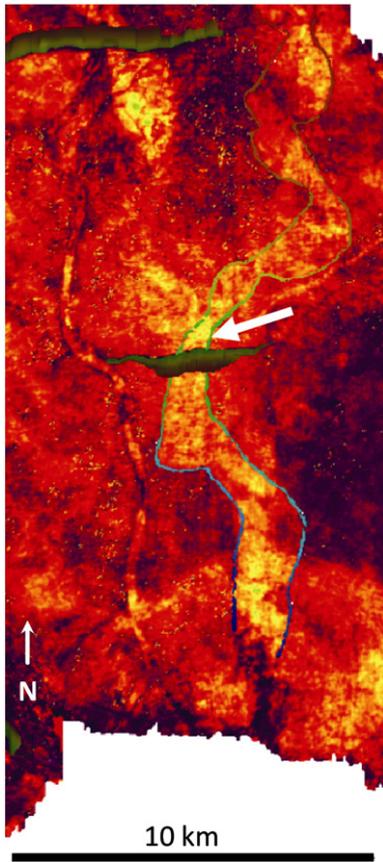
Fig. 15. Case C, a late Miocene channel-belt system (highlighted). View is from directly overhead with sweetness attribute shown. Hotter colors indicate higher values for the sweetness attribute. The arrow points to where the fault intersects the channel-belt.

across the fault. Total displacement across the fault is 52 m leading to an offset ratio of about 4%.

4.1.7. Case G

This south–southwest trending Pliocene channel-belt is located in the eastern portion of the survey and was mapped for over a 23 km distance (Fig. 19). The channel-belt crosses two southeast–northwest trending faults near the center of the mapped channel-belt. Within most of the channel-belt, the two faults are separated by only a few hundred meters and so are measured as a single faulting event. Upstream of the fault, the channel-belt approaches at an angle of 18° normal to the strike of the fault. Downstream of the fault, the channel-belt is oriented less than 1° normal to the strike of the fault. The average width is 3400 m and average thickness is 32 m. There is no systematic change in channel-belt geometry across the fault. The channel-belt intersects the faults at about 1400 m depth and is displaced a total of 96 m for an offset ratio of about 7%. This high offset ratio is a result of the channel-belt being displaced by both faults.

4.1.8. Case H

Case H is a Pliocene age south trending channel-belt located in the central portion of the dataset that has very low sinuosity at 1.03 over 10 km channel-belt distance (Fig. 20). The channel-belt crosses near the center of an east–west trending growth fault and positioning appears to be influenced by the fault. For one channel-belt width upstream of the fault, the channel-belt approaches at an angle of 24°
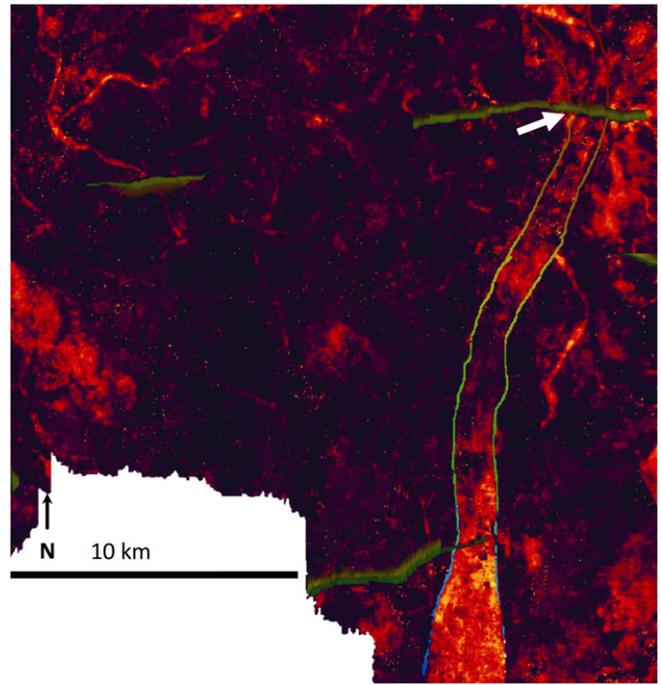

Fig. 16. Case D, a late Miocene channel-belt system (highlighted). View is from directly overhead on a map of the sweetness attribute. Hotter colors indicate higher sweetness values. The arrow points to where the fault intersects the channel-belt.

normal to the strike of the fault. For the same distance downstream of the fault, the channel-belt is oriented less than 1° from normal to the strike of the fault. Width increases from an average of 1600 m at the fault to 2 km approximately 1 km downstream of the fault. Average width for the entire mapped system is 1700 m. The
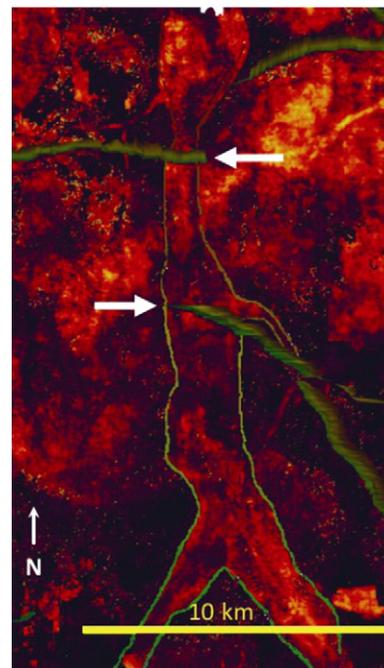

Fig. 17. Case E, a Mio-Pliocene channel-belt (highlighted). View is from directly overhead with sweetness attribute shown. Hotter colors indicate higher sweetness. The arrows point to where the faults intersect the channel-belt.
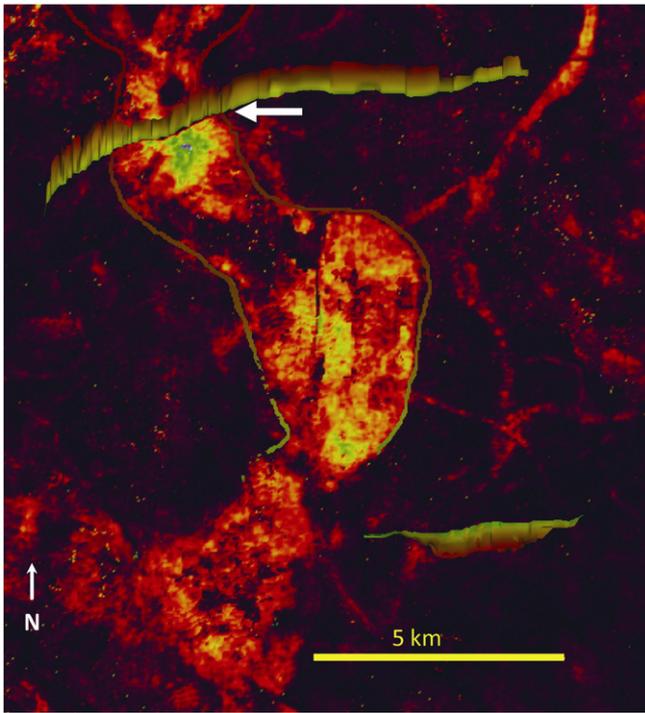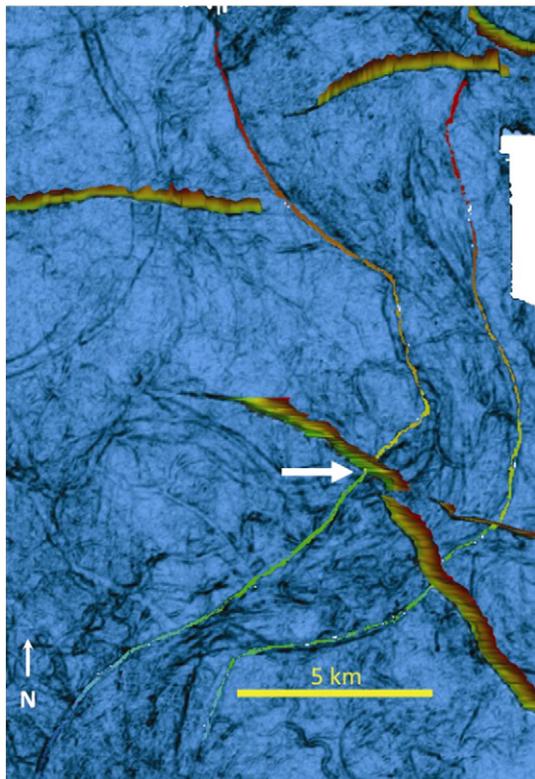
Fig. 18. Case F, a Mio-Pliocene channel-belt (highlighted). View is from directly overhead with sweetness attribute shown. Hotter colors indicate higher sweetness. The arrow points to where the fault intersects the channel-belt.

channel-belt crosses the central portion of the fault at a depth of about 920 m and is displaced 44 m leading to an offset ratio of 5.1%.

4.2. Channel-belt reorientation versus offset ratio

The channel-belt reorientation angle is plotted against faulting offset ratio in Fig. 21. The degree of channel-belt reorientation appears to increase with fault offset rate. This correlation is difficult to interpret because offset ratio is a cumulative measure of displacement on a growth fault, while a channel-belt will only respond to topographic relief across a fault during the time interval that it is active. Despite this shortcoming, the offset ratio does provide a standardized measure of overall faulting activity and we propose that higher values for the offset ratio are associated with greater likelihoods of significant fault-generated relief at any arbitrary time in the history of a fault.

4.3. Growth fault influence on the modern lower Mississippi River

Interestingly, the southeastern portion of the survey that contains the highest density of growth faults (a number of which affect the modern surface) corresponds to the last major channel bend on the Mississippi River before it reaches its Bird's Foot Delta. Fig. 22 shows a perspective view of the Mississippi River and the subsurface faults that extend to the modern surface, showing a one-to-one correlation between the positioning of a 13 km reach of the modern Mississippi River and the hanging walls of two adjacent growth faults. While correlation does not indicate causality, we propose that this sharp bend in the river is a product of channel redirection by active faulting. Unfortunately the high density and complex pattern of faulting in this area inhibit measuring any direct relationship between channel position and excess subsidence.

5. Discussion

In general, when a channel-belt emerges downstream of a fault, it is oriented roughly perpendicular to the strike of the fault. This has been demonstrated for seven channel-belts that intersect faults in
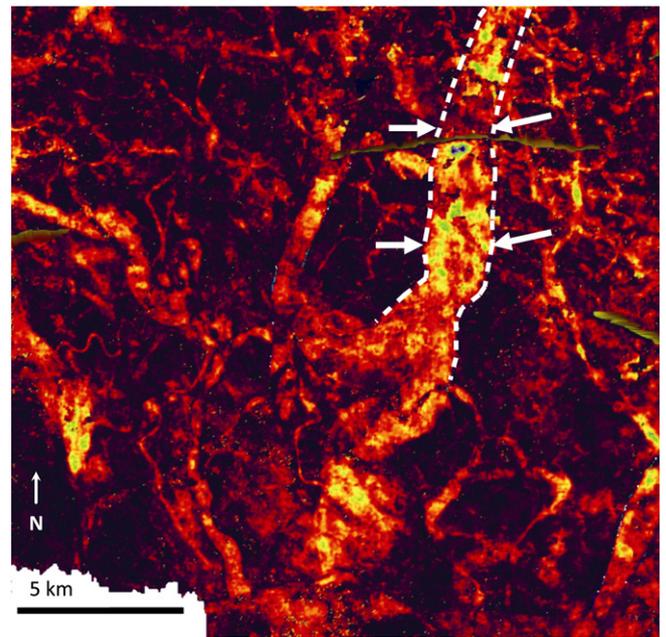

Fig. 19. Case G, a Pliocene channel-belt (highlighted). View is from directly overhead with similarity attribute shown. Darker colors indicate lower similarity. The arrow points to where the fault intersects the channel-belt.

Fig. 20. Case H, a Pliocene channel-belt (highlighted). View is from directly overhead with sweetness attribute shown. Hotter colors indicate higher sweetness. The north set of arrows points to the fault with the channel-belt imaged as the high sweetness area between both sets of arrows.
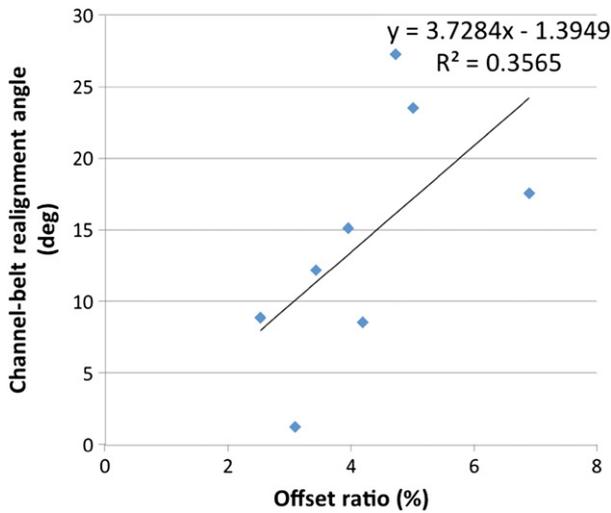
Fig. 21. Degree of channel-belt realignment by faults as a function of the fault offset ratio.
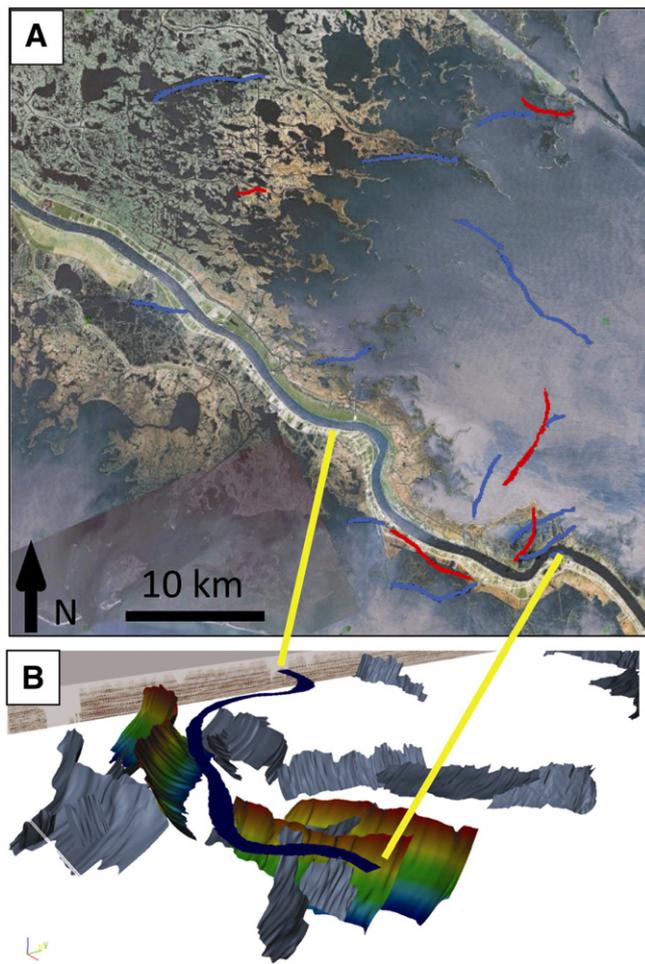
the lower Mississippi. In contrast, small channels (those with widths < 1 km) are rarely affected by faults. For over fifty examples of small channels within the dataset, only two are clearly redirected by faults. In addition, the small channels that are influenced by faults are not affected in the same way as larger channel-belts. Instead of an orientation perpendicular to the strike of the fault, as in channel-belts, small channels appear directed parallel to the strike of the fault along the zone of greatest fault displacement.

5.1. Timescales of avulsion and faulting

The potential for fluvial stratigraphy to be affected by faulting is interpreted mainly as a function of faulting timescale versus avulsion timescale. Long term (~10^5 years) vertical displacement rates for faults in this dataset are on the order of 10^{-2} mm/year (George, 2008). However, recent short-term displacement rates for these same faults can be significantly higher. For two faults within the survey bounds, Gagliano et al. (2003) reported displacements of up to 1.4 m over a two year time period. Rationalizing the short and long-term displacement rates on these same faults leads to a characteristic recurrence interval for punctuated, geologically instantaneous faulting on the order of 10^4 to 10^5 years (Fig. 23). If a fluvial system avulses more frequently than this, it is unlikely to be affected by faulting. While information on common avulsion frequencies for the late Miocene to Pliocene period studied is not available, avulsion frequencies ranging from 500 to 5000 years have been found for Holocene channels and delta lobes (Tornqvist, 1994).

Channel-belts are interpreted to be longer-lived features than small channels and as a result are less likely to avulse than small fluvial systems. These channel-belts are interpreted to be more likely to be influenced by faulting events than the smaller channels because of their lower mobility. The few small channels that are directed by faults most likely experienced a significant faulting event prior to avulsing.

5.2. Rollover towards a fault versus fluvial width

If a fluvial system is affected by a fault, what determines whether it will be directed parallel or perpendicular to the strike of the fault? The alteration of fluvial orientation across a fault can be interpreted as a function of the length scale for enhanced subsidence with distance from a fault (Fig. 24) and the channel or channel-belt width. Fault induced subsidence is highest at the fault and decreases to zero at some distance from the fault. This length scale tends to be on the order of a few hundred meters for faults in this dataset. The width of channel-belt systems can be over an order of magnitude larger
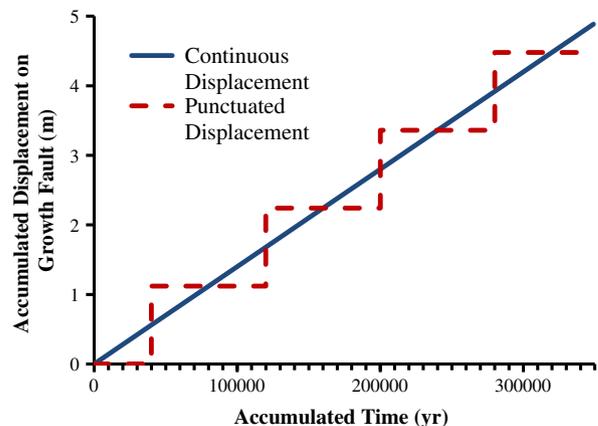

Fig. 22. (A): Projections of fault planes which appear to affect the modern surface of the Mississippi River Delta overlain on a satellite image; blue indicates a basinward fault dip and red indicates a landward dip. (B): Perspective view (from 3D seismic data) looking to the northwest of the planform of the modern Mississippi River (dark blue) with faults interpreted as affecting the modern surface highlighted (hotter colors are shallower). Deeper faults that do not appear to affect the surface are shown in solid light blue.

Fig. 23. Illustration of continuous fault displacement (blue line) with a rate of 0.014 mm/year versus punctuated displacement (red line) with an infrequently occurring ~1 m displacement.
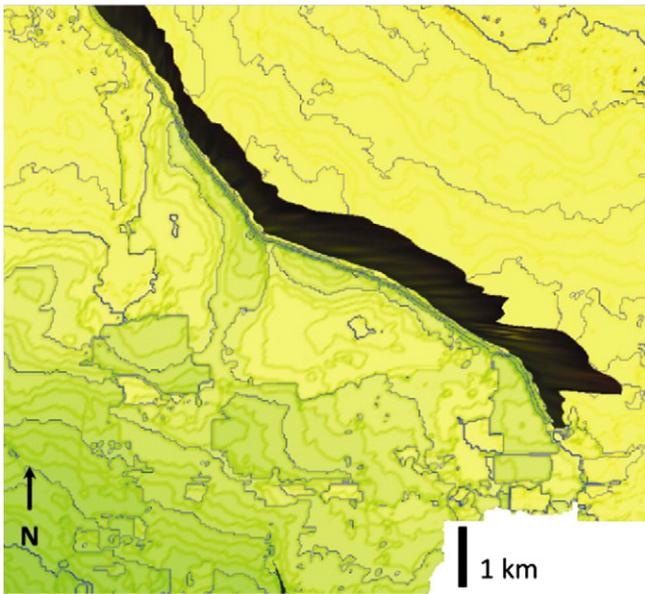
Fig. 24. Time map of surface around a fault (the fault is the dark shaded NW–SE oriented zone) with a 16 ms contour interval. The zone of enhanced, fault-created subsidence decreases to zero within ~500 m of the fault. Yellows indicate the shallowest parts of the mapped horizon.

than the length scale of fault displacement; because of this, channel-belts appear to be too large to be carried along the hanging wall of faults and instead emerge downstream oriented closer to perpendicular to the fault. The mechanism for this arrangement has not been identified, but the configuration likely represents the steepest line of decent across the faulted surface. Incised valley systems can be tens of kilometers wider than the width of growth faults and therefore appear to be too large to be affected by fault displacement events. Small channels, with widths similar to or less than the fault displacement length, do have the potential to be carried along the hanging wall of the fault if they experience a faulting event before avulsing.

In large scale, half-graben extensional settings, the subsidence length scale can be orders of magnitude greater than channel-belt width and so channel-belts are commonly carried along the zone of maximum subsidence. In the dataset used for this study, channel-belts are much wider than fault displacement lengths and channel depths are greater than relief generated by fault motion, so the traditional model is not appropriate. Fault displacement length scale, fluvial mobility, and channel width emerge as fundamental controls on the effectiveness and style of fault influence on fluvial stratigraphy.

6. Conclusions

1) On the hanging wall side of growth faults, the orientation of channel-belts appears to be affected by faulting. When a channel-belt approaches a fault at an oblique angle to the strike of the fault, the channel-belt tends to emerge downstream of the fault roughly perpendicular to the strike of the fault.

2) This channel-belt redirection by growth faults is loosely correlated with the offset ratio of the channel-belt. As offset ratio increases, the redirection of the channel-belt course appears to increase. However, if a channel-belt already approaches a fault close to perpendicular to the strike of the fault, realignment and apparent fault control will be low even with a high offset ratio.

3) The potential for growth fault influence on fluvial stratigraphy is related to the relative timescales of avulsion and faulting. Channel-belts are long lived features with avulsion timescales longer than faulting timescales. Channel-belts are more likely to

be influenced by faults than small channels with higher avulsion frequencies.

4) The style of fault control is dependent on the width of the fluvial system. The few small channels that are affected by faults are directed along the hanging wall of the fault. This is not seen in larger systems. Instead, channel-belt systems are directed perpendicular to the strike of the fault. This is likely a function of the fault displacement length compared to the width of the channel or channel-belt. Fluvial systems with small ratios (low channel width and high displacement length) are more likely to be steered along the hanging wall of the fault than perpendicular to the fault.

References

Alexander, J., Leeder, M.R., 1987. Active tectonic control on alluvial architecture. In: Ethridge, F.G., Flores, R.M., Harvey, M.D. (Eds.), Recent Developments in Fluvial Sedimentology: Contributions from the Third International Fluvial Sedimentology Conference Society of Economic Paleontologists and Mineralogists, Special Publication No. 39, pp. 243–252.

Bridge, J.S., Leeder, M.R., 1979. A simulation model of alluvial stratigraphy. Sedimentology 26, 617–644.

DeCelles, P.G., 1986. Sedimentation in a tectonically partitioned, nonmarine foreland basin: the Lower Cretaceous Kootenai Formation, southwestern Montana. Geological Society of America Bulletin 97, 911–931.

Gagliano, M.S., Burton Kemp III, E., Wicker, K.M., Wiltenmuth, K.S., Sabate, R.W., 2003. Neo-tectonic framework of southeast Louisiana and applications to coastal restoration. GCAGS/GCSSEPM Transactions 53, 262–276.

Gagliano, M.S., 2005. Effects of geological faults on levee failures in South Louisiana. In Testimony of Sherwood Gagliano. Ph.D. U.S. Senate Committee on Environment and Public Works, Senator James M. Inhofe, Chairman, Washington, D.C., pp. 1–28 (1, 10, 13, 14, 15, 25).

George, T., 2008. 3-D Seismic Evaluation of Fault Control on Quaternary Subsidence Patterns, Rates, and Related Surface Morphology in Southeastern Louisiana. The University of Texas at Austin 168 (MS Thesis).

Hickson, T.A., Sheets, B.A., Paola, C., Kelberer, M., 2005. Experimental test of tectonic controls on three-dimensional alluvial facies architecture. Journal of Sedimentary Research 75, 710–722.

Kim, W., Sheets, B.A., Paola, C., 2010. Steering of experimental channels by lateral basin tilting. Basin Research 22 (3), 286–301.

Mack, G.H., Leeder, M.R., 1999. Climatic and tectonic controls on alluvial-fan and axial-fluvial sedimentation in the Plio–Pleistocene Palomas half graben, southern Rio Grande rift. Journal of Sedimentary Research 69, 635–652.

Mack, G.H., Seager, W.R., 1990. Tectonic control on facies distribution of the Camp Rice and Palomas Formations (Pliocene–Pleistocene) in the southern Rio Grande rift. Geological Society of America Bulletin 102, 45–53.

Mackey, S.D., Bridge, J.S., 1995. Three-dimensional model of alluvial stratigraphy: theory and application. Journal of Sedimentary Research B65 (1), 7–31.

Maynard, J.R., 2006. Fluvial response to active extension: evidence from 3D seismic data from the Frio Formation (Oligo-Miocene) of the Texas Gulf of Mexico Coast, USA. Sedimentology 53 (3), 515–536.

Mohrig, D., Heller, P.L., Paola, C., Lyons, W.J., 2000. Interpreting avulsion process from ancient alluvial sequences: Guadalupe-Matarranya system (northern Spain) and Wasatch Formation (western Colorado). Geological Society of America Bulletin 112 (12), 1787–1803.

Mohrig, D., Straub, K.M., De la Rosa Illescas, A.C., 2010. When does spatial variation in subsidence rate influence the positioning of channels within Quaternary strata of the Mississippi River Delta? AAPG Annual Convention. April 11–14, 2010 — New Orleans, Louisiana, U.S.A., Search and Discovery Article #90104.

Nelson, T.H., 1991. Salt tectonics and listric-normal faulting. In: Salvador, A. (Ed.), The Gulf of Mexico Basin. Geological Society of America, the Geology of North America, v. J, pp. 73–89.

Peakall, J., 1998. Axial river evolution in response to half-graben faulting: Carson River, Nevada, U.S.A. Journal of Sedimentary Research 68, 788–799.

Peakall, J., Leeder, M.R., Best, J., Ashworth, P., 2000. River response to lateral ground tilting: a synthesis and some implications for the modeling of alluvial architecture in extensional basins. Basin Research 12, 413–424.

Straub, K., Paola, C., Mohrig, D., Wolinsky, M.A., George, T., 2009. Compensational stacking of channelized sedimentary deposits. Journal of Sedimentary Research 79, 673–688.

Taha, Z.P., Anderson, J.B., 2008. The influence of valley aggradation and listric normal faulting on styles of river avulsion: a case study of the Brazos River, Texas, USA. Geomorphology 95 (3–4), 429–448.

Tornqvist, T.E., 1994. Middle and late Holocene avulsion history of the River Rhine (Rhine–Meuse delta, Netherlands). Geology 22, 711–714.